

Detection prospects of light NMSSM Higgs pseudoscalar via cascades of heavier scalars from vector boson fusion and Higgs-strahlung

N.-E. Bomark^{a,b*}, S. Moretti^{c†}, L. Roszkowski^{b,d‡}

^aDepartment of Natural Sciences, University of Agder, Postboks 422, 4604 Kristiansand, Norway

^bNational Centre for Nuclear Research, Hoza 69, 00-681 Warsaw, Poland

^cSchool of Physics & Astronomy, University of Southampton, Southampton SO17 1BJ, UK

^dSchool of Physics & Astronomy, University of Sheffield, S3 7RH, UK

Abstract

A detection at the Large Hadron Collider of a light Higgs pseudoscalar would, if interpreted in a supersymmetric framework, be a smoking gun signature of non-minimal supersymmetry. In this work in the framework of the Next-to-Minimal Supersymmetric Standard Model we focus on vector boson fusion and Higgs-strahlung production of heavier scalars that subsequently decay into pairs of light pseudoscalars. We demonstrate that although these channels have in general very limited reach, they are viable for the detection of light pseudoscalars in some parts of parameter space and can serve as an important complementary probe to the dominant gluon-fusion production mode. We also demonstrate that in a Higgsfactory these channels may reach sensitivities comparable to or even exceeding the gluon fusion channels at the LHC, thus possibly rendering this our best option to discover a light pseudoscalar. It is also worth mentioning that for the singlet dominated scalar this may be the only way to measure its couplings to gauge bosons. Especially promising are channels where the initial scalar is radiated off a W as these events have relatively high rates and provide substantial background suppression due to leptons from the W . We identify three benchmark points that well represent the above scenarios. Assuming that the masses of the scalars and pseudoscalars are already measured in the gluon-fusion channel, the event kinematics can be further constrained, hence significantly improving detection prospects. This is especially important in the Higgs-strahlung channels with rather heavy scalars, and results in possible detection at 200/fb for the most favoured parts of the parameter space.

1 Introduction

The presence of an extra singlet superfield in the Next-to-Minimal Supersymmetric Standard Model (NMSSM) (see, e.g., [1] for a review) as compared to the MSSM, has a significant

*nilserik.bomark@gmail.com

†S.Moretti@soton.ac.uk

‡Leszek.Roszkowski@fuw.edu.pl

impact on the ensuing phenomenology of the Higgs sector at the Large Hadron Collider (LHC). In particular, the NMSSM Higgs sector is enlarged by two neutral mass eigenstates, one scalar and one pseudoscalar, in addition to the three MSSM-like ones.¹ The singlet nature of the scalar component of the additional superfield allows H_1 and A_1 to be very light when singlet dominated, even down to a few GeV, without entering into conflict with current theoretical and experimental constraints. This is so because their couplings to the fermions and gauge bosons of the SM are typically much smaller than those of the doublet-dominated Higgs bosons ($H_{2,3}$ and A_2), which are assumed heavier. As a consequence, the observation of any of these potentially light states, in addition to the SM-like Higgs boson already discovered at the LHC [2, 3], would constitute a hallmark signature of a non-minimal nature of supersymmetry (SUSY). Careful examination of their mass and coupling values in relation to the mass and coupling measurements of the 125 GeV SM-like Higgs boson (and possibly other discovered Higgs states) in a variety of production and decay channels will eventually enable one to profile their possible NMSSM nature.

The lightest pseudoscalar A_1 , in particular, can be the most crucial probe of the NMSSM as it can be very light, so that in principle it is accessible in meson decays, where it has been searched for initially [4, 5, 6, 7, 8, 9]. The A_1 state with mass $\gtrsim 5$ GeV has also been probed in the possible decay of a heavy (SM-like or not) scalar Higgs boson at LEP2 [10, 11] and Tevatron [12], where no significant excess was observed. Regarding the LHC, the situation is as follows. CMS searched for a light pseudoscalar produced either singly [13] or in pairs from the decays of a non-SM-like Higgs boson [14] and decaying into the $\mu^+\mu^-$ channel, while the $A_1A_1 \rightarrow 4\tau$ signature (via a SM-like Higgs decay) has been tackled in [15].² For completeness, let us also mention an ATLAS search for scalar particles decaying via narrow resonances into two photons in the mass range above 65 GeV [18], though this does not constrain light pseudoscalars very much.

In addition, there are plenty of phenomenological analyses aiming at assessing the scope of A_1 discovery within the NMSSM at the LHC. Prior to the SM-like Higgs boson discovery, quite some effort was put into extending the so-called ‘no-lose theorem’ of the MSSM — stating that at least one Higgs boson of the MSSM would have been discovered at the LHC via the usual SM-like production and decay channels throughout the entire MSSM parameter space [19] (see [20] for a recent review) to the case of the NMSSM [21, 22, 23, 24, 25, 26, 27, 28, 29, 30, 31, 32, 33, 34, 35, 36]. In the light of the recent Higgs boson discovery though, the above theorem is necessarily verified and, if one wants to prove the NMSSM to be a viable alternative to the MSSM, one ought to probe it away from the MSSM limit.

¹Hereafter, our book-keeping of the physical Higgs states of the NMSSM will be as follows: the CP-even states will be denoted by H_i (with $i = 1, 2, 3$ and such that $m_{H_1} < m_{H_2} < m_{H_3}$) while the CP-odd ones by A_i (with $i = 1, 2$ and such that $m_{A_1} < m_{A_2}$). We also use H_{SM} for the scalar playing the role of the discovered Higgs boson and H_S for the singlet dominated scalar.

²The sensitivity of the di-photon sample to a singly produced Higgs boson (of mass 150 GeV and above) decaying to $\gamma\gamma$ has also been investigated by CMS [16] alongside that of the $4b$ sample to pair production of 125 GeV Higgs bosons [17].

Following this line of reasoning, if one abandons the limiting case of SM-like decay channels of Higgs states, the NMSSM offers interesting signatures which are precluded in the MSSM after the latest experimental constraints, in the form of a variety of Higgs \rightarrow Two-Higgs and Higgs \rightarrow Gauge-Higgs decays. A large volume of phenomenological literature exists on these topologies, claiming that, for certain NMSSM parameter choices, these would be accessible at the LHC, eventually enabling one to disentangle the NMSSM from the MSSM hypothesis, thereby establishing a so-to-say ‘more-to-gain’ theorem [31]. The importance of such decays in the context of the NMSSM has been emphasised in Refs. [37, 38, 39] from the point of view of fine-tuning as well as a distinctive NMSSM signature at colliders. In particular, the $H_{1,2} \rightarrow A_1 A_1$ mode has received much attention. This decay can in fact be dominant in large regions of the NMSSM parameter space. It was realised that vector boson fusion (VBF) could be a viable production channel to detect the above modes at the LHC, in which the CP-odd Higgs pair decays into $jj\tau^+\tau^-$ [24, 25, 40] (where j represents a jet). Some scope could also be afforded by a 4τ signature in both VBF and Higgs-strahlung (HS) off-gauge bosons [28]. The gluon-fusion (GF) channel too could be a means of accessing $H_1 \rightarrow A_1 A_1$ decays, as long as the light CP-odd Higgs states both decay into four muons [30] or two muons and two taus [41]. Finally, the scope of NMSSM neutral Higgs boson production in association with $b\bar{b}$ pairs was assessed in [22, 33, 23, 42, 43, 44], including the case of $H_2 \rightarrow Z A_1$ decays with $Z \rightarrow jj$ and $A_1 \rightarrow \tau^+\tau^-$.

All the above mentioned analyses were, however, performed prior to the discovery of the Higgs boson at the LHC [3, 2]. In the aftermath of the discovery, detection prospects of all NMSSM Higgs bosons, including also via their decays into other Higgs states, were recently investigated in [45], though limited to the case of inclusive rates. Further, in [46], the $A_1 \rightarrow \gamma\gamma$ decay channel was studied in the regime of a light A_1 . In [47] it was then noted that in the NMSSM the A_1 could in fact be degenerate in mass with the SM-like Higgs boson H_{SM} . It could thus cause an enhancement in the Higgs boson signal rates near 125 GeV in the $\gamma\gamma$, $b\bar{b}$ and $\tau^+\tau^-$ channels simultaneously, provided that it is produced in association with a $b\bar{b}$ pair. The $b\bar{b}A_1$ channel was also studied in detail in [48], with a more optimistic conclusion as compared to [49]. In [50] the $H_{\text{SM}} \rightarrow A_1 A_1 \rightarrow 4\ell$ (with ℓ denoting e^\pm and μ^\pm) process at the LHC was studied in detail, while the $b\bar{b}\mu\mu$ final state was deemed the most promising in [51]. The production of A_1 via neutralino decays has also been recently revisited in [52, 53, 54]. Finally, NMSSM benchmark proposals capturing much of this phenomenology exist in the literature [35, 55].

In this work we continue to pursue a recently started endeavour [49], with an intention to systematically analyse all the production and decay processes that could potentially lead to the detection of a light NMSSM A_1 at the LHC with $\sqrt{s} = 14$ TeV. In [49] (see also [56, 57]), we considered the case of the light pseudoscalar A_1 produced from a heavy Higgs boson coming from GF which then decays into either A_1 pairs or $Z A_1$ (with the Z in turn decaying into electrons/muons). We found that the A_1 can be accessible through a variety of signatures proceeding via $A_1 \rightarrow \tau^+\tau^-$ and/or $b\bar{b}$, the former assuming hadronic

decays and the latter two b -tags within a fat jet or two separate slim ones. Some of these channels were also studied in the comprehensive review of exotic Higgs decays contained in [58].

In the present paper, working under the assumption that a light A_1 state has been found through one or more of the decay channels analysed in [49], we assess the scope of the LHC Run II in profiling its nature by resorting instead to the VBF and HS Higgs production modes. This would then enable access to the heavy Higgs couplings to both charged and neutral gauge bosons, thus complementing the GF channel which only allows one to measure their fermion couplings. It is worth emphasising that for the non-SM-like scalars, this might be the only chance to access these couplings as the decay to pairs of pseudoscalars can be completely dominating. Furthermore, although the VBF and HS channels have significantly smaller cross sections than GF, the improved possibilities for tagging through the additional (forward/backward) jets for VBF and the additional leptons from vector boson decays in HS, may still render them competitive against GF, for which many of the triggers needed for fully hadronic final states have been scarcely tested in the experimental environment. In view of this, in this paper we perform a preliminary study of light A_1 s in the VBF and HS Higgs production modes by making some simplifying assumptions, in particular by ignoring detector effects and trigger thresholds.

Before plunging into the details of this new analysis, we should also point out here that in the NMSSM both H_1 and H_2 , the lightest and next-to-lightest CP-even Higgs bosons, respectively, can alternatively play the role of the SM-like Higgs boson H_{SM} , as emphasised already in [59, 60, 61, 62, 63] and confirmed in [49, 56, 57].

The article is organised as follows. In section 2, we define the parameter space of the NMSSM under consideration. In section 3 we explain our approach to scan the NMSSM parameter space while in section 4 we describe our signal-to-background analyses. Then in sections 5, 6 and 7 we discuss in detail our results for VBF and HS (the latter separately for the neutral (ZH) and charged (WH) channels) at the LHC over the entire NMSSM parameter space. Then, after presenting some benchmark points available for experimental investigation in section 8 and testing them at the CERN pp machine, we afford a brief digression on the physics of a light A_1 state at a future e^+e^- collider (in section 9). We summarise and conclude in section 10.

2 The NMSSM parameter space

The idea behind the NMSSM is to explain the peculiar feature of the MSSM that the supersymmetry preserving μ term is phenomenologically required to be of the same scale as the soft supersymmetry breaking mass parameters, while in principle it would be expected to be of a completely different origin.

In the NMSSM this so-called μ problem is solved by introducing an extra gauge-singlet chiral superfield \hat{S} whose scalar component receives a vacuum expectation value (VEV)

due to its soft supersymmetry breaking terms. All that is needed to generate an effective μ term of the same order as the soft supersymmetry-breaking parameters, is then to have a term $\lambda \widehat{S} \widehat{H}_u \widehat{H}_d$ in the superpotential and the (effective) μ term $\mu_{\text{eff}} \equiv \lambda s$ will be given by the VEV of S times the coupling constant λ . We also need to add a cubic term in \widehat{S} to the superpotential, so that the terms involving \widehat{S} read

$$\lambda \widehat{S} \widehat{H}_u \widehat{H}_d + \frac{\kappa}{3} \widehat{S}^3, \quad (1)$$

where λ and κ are dimensionless coupling constants. Further, one needs to add the corresponding soft supersymmetry breaking terms in the scalar potential. The soft supersymmetry breaking terms relevant for the Higgs sector are:

$$m_{H_u}^2 |H_u|^2 + m_{H_d}^2 |H_d|^2 + m_S^2 |S|^2 + (\lambda A_\lambda S H_u H_d + \frac{\kappa}{3} A_\kappa S^3 + h.c.), \quad (2)$$

where m_{H_u} , m_{H_d} , m_S , A_λ and A_κ are dimensionful mass and trilinear parameters. By minimising the scalar potential we can trade the three scalar mass parameters for μ_{eff} and $\tan \beta$ (i.e., the ratio between the VEVs in the up type and down type Higgs doublets, v_u/v_d). We also replace A_κ with M_p , the singlet pseudoscalar mass entry; if input is given at the Electroweak scale, this is close to the lightest pseudoscalar mass which improves the efficiency of the scan. For this reason we use parameters defined at the EW scale throughout the paper.

For the sfermion masses we use a common mass parameter m_0 and for all gaugino masses we use a common parameter $m_{1/2}$ but to take into account the effects of running from a high scale unification we use $M_2 = m_{1/2}$, $M_1 = m_{1/2}/2$, $M_3 = 3m_{1/2}$. Similarly, we use a common parameter A_0 for all trilinear parameters except A_λ and A_κ . Since the most significant effect these parameters have on the Higgs sector is radiative corrections to the Higgs mass, unifying them in the above manner should not impact much on the observables of interest, thus giving maximum freedom in the Higgs sector while keeping the number of free parameters at a manageable level. This leaves us with nine parameters:

$$m_0, m_{1/2}, A_0, \tan \beta, \mu_{\text{eff}}, \lambda, \kappa, A_\lambda, M_p. \quad (3)$$

As can be seen in the tree-level mass for the lightest doublet scalar, i.e. essentially (up to mixing with the singlet scalar) H_{SM} in the NMSSM [1],

$$m_{H_{\text{SM}}}^2 \simeq m_Z^2 \cos^2 2\beta + \lambda^2 v^2 \sin^2 2\beta, \quad (4)$$

there is an additional contribution to the Higgs mass coming from the λ term, not present in the MSSM. This means that, when this term is sizeable, i.e., when λ is large and $\tan \beta$ is small, one can obtain the measured 125 GeV mass without resorting to large radiative corrections from the stop sector, which is necessary in the MSSM. In the forthcoming sections we will refer to this part of parameter space as the ‘naturalness limit’. Also notice that, when $H_2 = H_{\text{SM}}$, it is possible that some mixing between H_1 and H_2 increases m_{H_2} further, hence making it even easier to achieve (and indeed exceed) the required 125 GeV [59, 64, 65, 66, 67, 68].

3 The scans

In order to investigate the prospects of the discussed channels in the NMSSM we performed a number of Bayesian scans of the above mentioned 9-dimensional parameter space. These scans use MultiNest-v2.18 [69] for nested sampling of the parameter space and NMSSMTools-v4.6.0 [70], including the bug-fix of version 4.7.1, for the calculation of the Higgs mass spectrum, couplings, Branching Ratios (BRs) and constraints on the parameter points (including LEP-II bounds on light scalars and pseudoscalars). The output from NMSSMTools is further processed by HiggsBounds-v4.1.3 [71, 72, 73, 74] to ensure against exclusion from searches for other Higgs bosons. Also SuperIso-v3.3 [75] is used to calculate b -physics variables. These are then required to comply with the constraints from [76] (in all cases, the last number refers to a theoretical uncertainty in the numerical evaluation):

- $\text{BR}(B_s \rightarrow \mu^+ \mu^-) = (3.2 \pm 1.35 \pm 0.32) \times 10^{-9}$,
- $\text{BR}(B_u \rightarrow \tau \nu) = (1.66 \pm 0.66 \pm 0.38) \times 10^{-4}$,
- $\text{BR}(\bar{B} \rightarrow X_s \gamma) = (3.43 \pm 0.22 \pm 0.21) \times 10^{-4}$.

To guard against over-closure of the Universe, an upper bound of $\Omega_\chi h^2 < 0.131$ on the dark matter relic density was also applied. This was set assuming a 10% theoretical error on the central value of 0.119 from PLANCK [77] and the relic density was calculated with the help of MicrOMEGAs-v2.4.5 [78]. We do not include any constraint on $(g-2)_\mu$; the contributions here are always too small to cause problems, they are actually too small to reconcile the experimental value with the Standard Model calculations.

A total of four scans were run; two where either one of H_1 and H_2 was allowed to be the SM-like one, and since this mostly gave points with $H_1 = H_{\text{SM}}$, two other scans were run including a bias towards $H_2 = H_{\text{SM}}$. In both cases did we use one scan focusing on the naturalness limit and one wider scan. The parameter ranges for all scans are given in table 1, where the reduced range focuses on the naturalness limit and, since the couplings relevant to e.g., $H_i \rightarrow A_1 A_1$ decays depend on λ this is the most promising part of parameter space to look for these channels. All the scan results are then combined into two samples, one with $H_1 = H_{\text{SM}}$ and one with $H_2 = H_{\text{SM}}$.

For all samples we require $m_{H_{\text{SM}}}$ to lie between 122 and 129 GeV. The best experimental values of the Higgs mass are 125.03 GeV from CMS [79] and 125.36 GeV from ATLAS [80] with uncertainties of the scale of a fraction of a GeV, however, to allow for potentially large theoretical uncertainties, we allow a significantly larger range. Note, though, that the benchmark points of section 8 are within the experimental limits.

The scans also contain a bias towards low pseudoscalar masses (favouring $m_{A_1} \lesssim 65$ GeV, but allowing m_{A_1} up to 140 GeV) and SM-like signals rates for H_{SM} . These constraints are implemented to ensure that the scans do not waste too much time exploring uninteresting parts of parameter space. Conversely, they should not exclude any points that might be of interest for further investigation.

Parameter	Extended range	Reduced range
m_0 (GeV)	200 – 2000	200 – 2000
$m_{1/2}$ (GeV)	100 – 2000	100 – 1000
A_0 (GeV)	–5000 – 5000	–3000 – 3000
μ_{eff} (GeV)	50 – 1000	100 – 200
$\tan \beta$	1 – 30	1 – 6
λ	0.01 – 0.7	0.4 – 0.7
κ	0.01 – 0.7	0.01 – 0.7
A_λ (GeV)	200 – 2000	200 – 1000
M_p (GeV)	3 – 140	3 – 140

Table 1: Parameter ranges used in the scans. The reduced range focuses on the naturalness limit.

Though similar scans were also performed in our previous paper [49], there are a number of important updates. Apart from updated versions of some of the software (most importantly NMSSMTools), the most notable difference is the treatment of the constraints on signal rates for H_{SM} ; this is now done using the built in constraints of NMSSMTools, which uses constraints obtained from Lilith 1.0 [81]. Especially important is the inclusion of signal constraints on $H_{\text{SM}} \rightarrow b\bar{b}$; it turns out that virtually all points in the naturalness limit with $m_{A_1} < m_{H_{\text{SM}}}/2$ are excluded by this constraint. Given the poor measurement of this channel as compared to e.g. $H_{\text{SM}} \rightarrow \gamma\gamma$ and $H_{\text{SM}} \rightarrow ZZ$, this might sound surprising, but it turns out that the latter channels can afford a relatively large $\text{BR}(H_{\text{SM}} \rightarrow A_1 A_1)$ by compensating with larger branching ratios for the measured channels, this however is not possible for $H_{\text{SM}} \rightarrow b\bar{b}$ since this branching ratio cannot be further increased and points with increased vector boson channels tend to have some singlet component in the H_{SM} which further reduces the production cross-section and therefore conflicts with $H_{\text{SM}} \rightarrow b\bar{b}$. In the case of $H_1 = H_{\text{SM}}$ this only confirms the picture from [49] where only a wider scan yields points below $H_{\text{SM}}/2$. For $H_2 = H_{\text{SM}}$ on the other hand, this makes a big difference; while our previous studies deemed $H_1 \rightarrow A_1 A_1$ with $H_2 = H_{\text{SM}}$ a very promising channel, this has now changed.

To illustrate the difference, we plot in figure 1 the same sensitivity curves as in figure 12(a) of [49] but with our new scans instead. It is clear that, while the earlier scan found good chances of discovery already at 30/fb the prospects are now looking far dimmer. If we look at λ as a function of m_{A_1} as is done in figure 2, we see clearly that it is the high λ region that is unreachable for $m_{A_1} < m_{H_{\text{SM}}}/2$, in this region the presence of the $H_{\text{SM}} \rightarrow A_1 A_1$ channel suppresses the signal rates of H_{SM} , especially for large λ (the relevant $H_{\text{SM}} A_1 A_1$ coupling contains a factor λ^2); for the vector boson channels this can be somewhat compensated by giving a somewhat larger singlet component to the H_{SM} ,

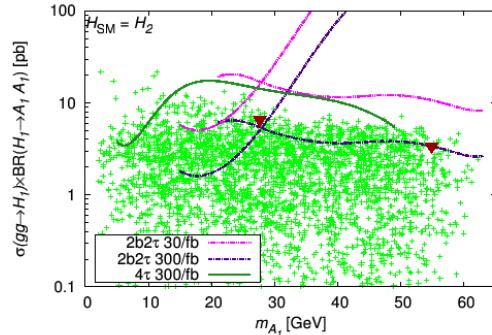


Figure 1: The sensitivity in the previously most promising channel with $gg \rightarrow H_1 \rightarrow A_1 A_1$ with $H_2 = H_{SM}$, sensitivity curves are identical to the ones in figure 12(a) of [49]. The sensitivity curves correspond to the one fat jet plus two τ -jets (the curves at low m_{A_1}) and the two single b-jets plus two τ -jets (the curves at higher m_{A_1}) analyses. For the fat jet plus two τ -jets $m_{H_1} = 100$ GeV, while for the two b-jets plus two τ -jets curve $m_{H_1} = 125$ GeV, which allows the coverage of points with large m_{A_1} . The green points comply with all constraints of our scans. The red triangles mark the benchmark points defined in section 8.

this reduces the production cross section but also the width of competing decay channels hence increasing the signal rate for the vector boson channels; however, this cannot be done simultaneously for $H_{SM} \rightarrow b\bar{b}$. With these updated constraints $\text{BR}(H_{SM} \rightarrow A_1 A_1)$ never reaches more than just above 20%.

It is also worth mentioning that compared to the scans of [49], we here use somewhat different parameters, especially, we use the singlet pseudoscalar mass term, M_p , as input (to improve efficiency) and all input is at the EW scale (a necessity if M_p is to actually correspond to m_{A_1}). We also use the full NNLO contributions to the scalar masses in NMSSMTools, in contrast to what was done in [49]. This raises the $m_{H_{SM}}$ especially for large stop mixing and mass, and might therefore further favour points with large $m_{H_{SM}}$ contributions from the stop sector rather than the NMSSM specific contributions of the naturalness limit.

Finally, in both figure 2(a) and (b), there is a depletion of points above 70–80 GeV: this is due to the bias towards low m_{A_1} included in the scans.

Given the requirement of SM-like signal rates for H_{SM} , it is natural that its reduced coupling to vector bosons will always be large (close to 1). The reduced coupling of H_S will be smaller but can, due to mixing, still be significant, however the reduced coupling of H_3 always turns out very small.

To understand this let us look at the couplings of interest: they both have a factor [1]

$$(v_d S_{31} + v_u S_{32}), \quad (5)$$

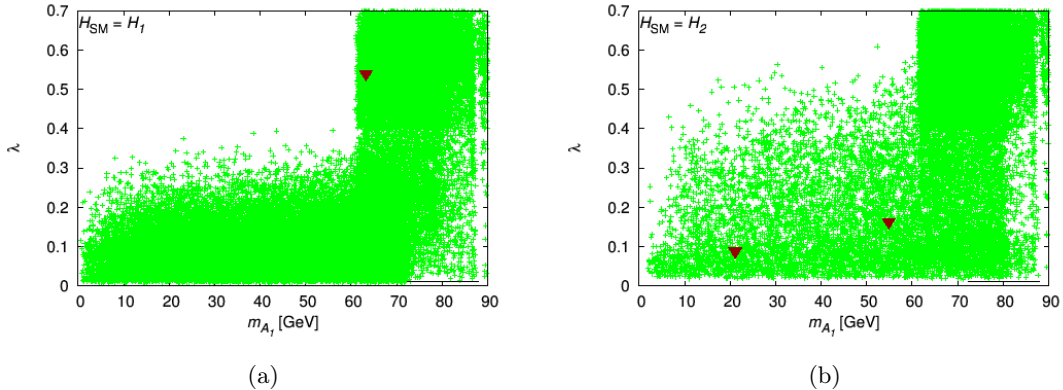


Figure 2: The parameters λ versus m_{A_1} . The colour code for the points is the same as in figure 1.

where S_{31} and S_{32} are elements of the neutral scalar mixing matrix, defined as $H_i = S_{ij}H_j^{\text{Weak}}$ with $H_j^{\text{Weak}} = (\Re(H_d), \Re(H_u), \Re(S))$. We know that $v_u/v_d = \tan\beta$ by definition and, due to the structure of the mixing matrices, it turns out that $S_{31}/S_{32} \approx -\tan\beta$. Hence the factor (5) becomes small; typically, the reduced coupling tends to be ≈ 0.01 or smaller and, since it comes squared in the production cross sections for both VBF and HS, we get a suppression factor of at least 10^{-4} , rendering these channels useless for H_3 . Note that the cancellation mentioned above gives a much stronger suppression than naively expected from the fact that H_{SM} has to have SM-like couplings combined with the sum-rule requiring the sum of the squares of the vector boson couplings for all three scalars to be unity.

4 Event analyses

Since the vector boson couplings to H_3 are always very small we do not consider channels including H_3 production here, they do not have big enough cross sections to be of any interest. Furthermore, since the channels $H_{1,2} \rightarrow A_1 Z$ were shown in [49] to be very difficult, we here focus only on the $H_{1,2} \rightarrow A_1 A_1$ channels. Given the lower cross sections for VBF and HS production as compared to GF, none of the other channels carry promise for detection.

To estimate the sensitivity in the channels of interest we use MadGraph5_aMC@NLO [82], employing default parton distribution functions and factorisation and renormalisation scales, to generate the relevant backgrounds. Hadronisation and signal generation is then done using Pythia 8.180 [83], while jet clustering and jet substructure studies are done using FastJet-v3.0.6 [84].

The production cross sections for the signals are calculated using tabulated cross sections for the SM Higgs, taken from [85], together with reduced couplings for the relevant scalar from NMSSMTools.

For all final state objects we use the following acceptance cuts:

- $|\eta| < 2.5$ for all final state objects,
- $p_T > 15$ GeV for all final state jets (τ -jets, b -jets and light-quark jets),
- $p_T > 10$ GeV for all final state leptons (e^\pm , μ^\pm),
- $\Delta R \equiv \sqrt{(\Delta\eta)^2 + (\Delta\phi)^2} > 0.2$ for all b -quark pairs,
- $\Delta R > 0.4$ for all other pairs of final state objects,

where p_T , η , ϕ are the transverse momentum, pseudorapidity and azimuthal angle, respectively. Both B -mesons and τ s are decayed by Pythia and the decay products included in the jet clustering in FastJet. The identification of b - and τ -jets is then done by tracing the jet constituents back in the event record, thereby identifying b - and τ -jets as jets where most of the constituents are decay products from B -mesons and τ s respectively. On top of this the event sample is rescaled by an assumed tagging efficiency of 50% for each b - and τ -jet. This efficiency is somewhat conservative (c.f. [86, 87]) but this is motivated by our soft signals. No knowledge about the charge of the jets is assumed. For the $t\bar{t}$ background for the WH channel, we assume a 1% mistagging probability for light jets.

For the VBF backgrounds the two additional light jets are required to satisfy the following criteria:

- $|\eta| < 5$,
- $p_T > 30$ GeV,
- $\Delta R > 3$,
- $M_{jj} > 300$ GeV,

where M_{jj} is the invariant mass of the two forward/backward jets. (Due to numerical difficulties in producing enough statistics, somewhat harder cuts, $M_{jj} > 500$ GeV and $p_T > 40$ GeV, are imposed on the parton level production in the $4b$ final state.) In addition, the jets are required to be located in the opposite hemispheres (i.e. one positive and one negative η) and there should be no other jet (apart from the signal objects) with $p_T > 30$ GeV between (in terms of η) the two jets.

The cross sections for the dominant backgrounds after the above acceptance cuts are applied, are given in table 2. Note that for the $0j$ and $1j$ backgrounds the above VBF specific cuts are not applied, hence the much larger cross-sections, this will be compensated by smaller acceptance after hadronisation. After hadronisation and jet clustering the final

Channel	Parton level cross section
VBF	
$2j + 4b$	72 pb
$0j + 2b2\tau$	3.1 pb
$1j + 2b2\tau$	3.2 pb
$2j + 2b2\tau$	0.19 pb
$0j + t\bar{t}$	597 pb
$1j + t\bar{t}$	845 pb
$2j + t\bar{t}$	80 pb
ZH	
$Z + 4b$	0.31 pb
$Z + 2b2\tau$	2.7 fb
WH	
$W + 4b$	36 fb
$t\bar{t}b\bar{b}$	4.0 pb
$t\bar{t}$	597 pb

Table 2: Background cross sections for the dominant backgrounds at parton level as calculated by MadGraph.

VBF cuts are applied to the real jets (as opposed to the parton as done above) and then $M_{jj} > 500$ GeV and $p_T > 40$ GeV are required for all signal and background in the VBF channels. For the rest of the paper, in all discussions of VBF production $t\bar{t}$ refers to the sum of $0j + t\bar{t}$, $1j + t\bar{t}$ and $2j + t\bar{t}$ and $2b2\tau$ refers to the sum of $0j + 2b2\tau$, $1j + 2b2\tau$ and $2j + 2b2\tau$. The total background for the $2b2\tau$ channel is the sum of $t\bar{t}$ and $2b2\tau$. We do not include further backgrounds in the $4b$ channel since this channel is in any case inferior to $2b2\tau$ and therefore of little interest.

In order to optimise the sensitivity to boosted A_1 s we employ the jet substructure method of [88] (see also [49] for further details). This gives us fat jets that we assume to originate from an A_1 decaying into a $b\bar{b}$ pair. To avoid contamination from single b -jets, we require all fat jets to have $p_T > 30$ GeV and invariant mass > 12 GeV.

For each event with the proper final state we look for two A_1 candidates (either one fat jet, two b -jets or two τ -jets depending on which channel we are looking at) and compare their respective invariant mass: if they are within 15 GeV of each other we accept that event and if, in addition, the combined invariant mass of the two candidates is within 125 ± 30 GeV, it is accepted as an event where an H_{SM} was produced and decayed into two A_1 s. In all the channels we perform two analyses in parallel: one with the jet substructure method, where only fat jets and no single b -jets are used, and one where no jet substructure is exploited but only single b -jets are used. For the four b -jet final state we check all combinations of

b -jet pairs and accept the first one with both invariant masses within 15 GeV of each other.

To obtain the sensitivity for a given m_{A_1} we then count the events where the A_1 candidates masses are within 15 GeV of the mass m_{A_1} and can then calculate — for a given luminosity, \mathcal{L} — how large a signal cross section is needed to obtain a significance $S/\sqrt{B} > 5$ where S is the number of signal events and B is the background. In all channels we require at least 10 events in order to claim discovery, so if $S/\sqrt{B} > 5$ is fulfilled for $S < 10$, we instead use $S > 10$ as the limiting sensitivity. This means that, in channels with very low background, the sensitivity is $\propto \mathcal{L}$ rather than $\propto \sqrt{\mathcal{L}}$ as is the case for S/\sqrt{B} .

We will be studying the VBF and HS channels in turn, splitting the latter into the ZH and WH modes. For the sensitivity curves in the forthcoming sections, we limit ourselves to scalar masses up to 175 GeV, there is no problem in principle to employ these analyses at higher masses, they would actually gain some sensitivity with harder objects to study, but the production cross-section for the initial scalar also drops fast with increasing mass, hence prohibiting any discovery prospects.

5 VBF

The backgrounds used in the analysis of the VBF mode are irreducible, i.e., $4b+2$ jets and $2b2\tau+2$ jets. In addition, we include the $t\bar{t}+2$ jets — with both W s from the top quarks decaying to τs — in the $2b2\tau$ channel. Since the latter turns out to be the dominant background in this channel, we also invoke a cut on Missing Transverse Momentum (MET) to reduce it.

This cut requires that the p_T of the two τ -jets combined should be larger than the total MET of the event. This reduces the $t\bar{t}+2$ jets background by a factor 2-3 while leaving both signal and irreducible backgrounds virtually intact. Note, however, that the MET here is simply the sum of the momentum of all invisible particles (i.e., neutrinos), a full detector simulation with mis-measured/missing jets, pile-up etc. would be necessary to fully determine the true effectiveness of this cut. This latter cut, though effective, is, however, not crucial for the usefulness of this analysis.

Figure 3 shows the discovery reach in the interesting channels for 3000/fb of integrated luminosity and using the overall constraint that the total four-body invariant mass should be 125 ± 30 GeV. It is clear that the $2b2\tau$ channels are the most promising ones and hence we will not consider the $4b$ channels in the following. All sensitivity curves have been rescaled by a factor $1/0.9$ for each $b\bar{b}$ pair in the final state and a factor $1/0.1$ for each $\tau\tau$ pair in the final state, to allow for a direct comparison of the sensitivity to $\sigma(q\bar{q} \rightarrow q\bar{q}H_i) \times \text{BR}(H_i \rightarrow A_1A_1)$. As expected, we see in figure 3 that the jet substructure analysis only works well for rather low m_{A_1} .

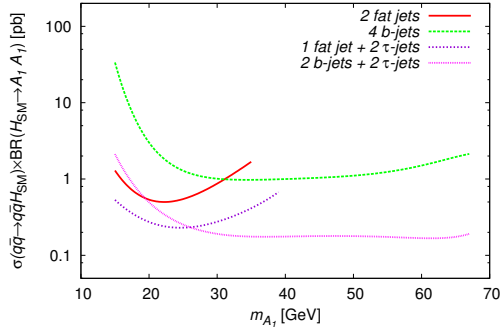


Figure 3: Sensitivity for the $4b$ and $2b2\tau$ channels in VBF production. All curves assume 3000/fb of integrated luminosity and use $m_{H_i} = 125$ GeV and the corresponding cut on the total final state invariant mass.

5.1 H_1 SM-like

To illustrate the reach of the LHC in these channels, in figure 4 we compare the sensitivity with the points from our scans when $H_1 = H_{SM}$. In figure 4(a), we show sensitivity curves using a 125 GeV Higgs (and employing the corresponding constraint), always using the best out of the 2 b -jets and fat jet analyses. As is clearly seen, the prospects for $H_1 \rightarrow A_1 A_1$ will always be rather limited due to the small number of points in the interesting region of parameter space. It is clear that the points never reach above 1 pb, this is a direct effect of the constraints on the signal rates of H_{SM} , higher $BR(H_{SM} \rightarrow A_1 A_1)$ would necessarily suppress other channels unacceptably much. This means that we need 3000/fb to discover something and our best chance would be the low mass region where the jet substructure methods can improve sensitivity.

As regards the $H_2 \rightarrow A_1 A_1$ channel, it is somewhat easier to find acceptable points just above the $m_{A_1} < m_{H_1}/2$ threshold, however, they do not reach much higher in terms of rates. This can be seen in figure 4(b), where the prospects for $H_2 \rightarrow A_1 A_1$ are illustrated. Figure 4(b) uses sensitivity curves for $m_{H_2} = 175$ GeV in order to cover the whole interesting parameter space. Also, here do we always employ the analysis (with or without jet substructure) with the best sensitivity. The smallness of the rates also above the kinematic threshold is a consequence of the requirement that H_{SM} has to have very SM-like couplings to meet the signal rate constraints, and hence H_2 has to be very singlet-like and hence have very small production rates even if the $H_1 \rightarrow A_1 A_1$ channel is kinematically closed. In the end this means that our best chance also in this channel seems to be the light pseudoscalars where jet substructure is useful.

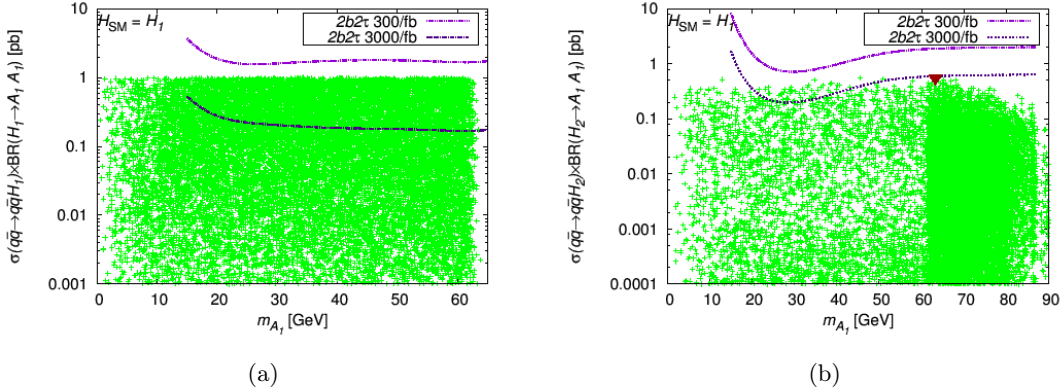


Figure 4: LHC reach in $H_1 \rightarrow A_1 A_1$ (left) and $H_2 \rightarrow A_1 A_1$ (right) for $H_1 = H_{\text{SM}}$ in the VBF channel. In panel (a) the sensitivity curves use $m_{H_1} = 125$ GeV, while (b) uses $m_{H_2} = 175$ GeV and both uses the best of the 2 b -jets and fat jet analyses. The colour code for the points is the same as in figure 1.

5.2 H_2 SM-like

As mentioned before, after the inclusion of especially the signal rate constraint on $H_{\text{SM}} \rightarrow b\bar{b}$, the case $H_2 = H_{\text{SM}}$ does not differ so much from $H_1 = H_{\text{SM}}$. In figure 5(a) we show the sensitivity for $H_1 \rightarrow A_1 A_1$, both with jet substructure using $m_{H_1} = 100$ GeV and without jet substructure using $m_{H_1} = 125$ GeV, but without constraining the four-body invariant mass. We use two separate curves since they use different m_{H_1} . The use of $m_{H_1} = 100$ GeV is motivated by the typical values of m_{H_1} while 125 GeV is needed to cover the whole range of m_{A_1} , the $m_{A_1} = 100$ GeV curve would be kinematically cut off at $m_{A_1} = 50$ GeV. Also in this channel we will need 3000/fb to see something.

From figure 5(a) it even looks like the jet substructure does worse than the simpler 2 b -jet analysis, though one should remember that these curves uses different m_{H_1} ; the lower m_{H_1} of the fat jet analysis means decreased sensitivity. For the $4b$ final state this can be compensated by an improved sensitivity due to the fat jet analysis, however, as can be seen in figure 3, the low mass improvement with the fat jet analysis is not as great for $2b2\tau$ as it is for $4b$, leading to comparatively poor sensitivity to $m_{A_1} \approx 20$ GeV in figure 5(a).

In figure 5(b) we show the sensitivity in the $H_2 \rightarrow A_1 A_1$ channel using $m_{H_2} = 125$ GeV and requiring the four-body invariant mass to be 125 ± 30 GeV. For all points along the sensitivity curves we use the analysis that gives the best sensitivity (with or without jet substructure). As expected, this is very similar to figure 4(a) with a clear upper limit for the rate at 1 pb stemming from the signal rate requirements on H_{SM} .

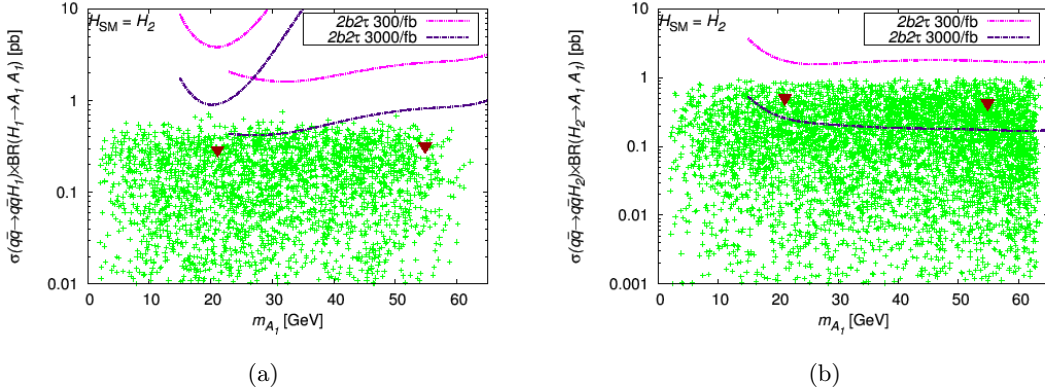


Figure 5: LHC reach in $H_1 \rightarrow A_1 A_1$ (left) and $H_2 \rightarrow A_1 A_1$ (right) for $H_2 = H_{\text{SM}}$ in the VBF channel. The sensitivity curves in panel (a) correspond to the one fat jet (the curves at low m_{A_1} using $m_{H_1} = 100$ GeV) and the two single b-jets (the curves at higher m_{A_1} using $m_{H_1} = 125$ GeV) analyses. In panel (b) $m_{H_2} = 125$ GeV is used along with the best of the 2 b-jets and fat jet analyses. The colour code for the points is the same as in figure 1.

6 Higgs-strahlung via ZH

With an additional Z boson, triggering and background suppression is much improved. To extract the signal we only use leptonically decaying Z bosons. This means, that in addition to acceptances, we require one di-lepton pair with invariant mass 90 ± 10 GeV. This is very powerful in suppressing the backgrounds, however, the small leptonic BR of the Z together with the small production cross sections in the ZH channel, means that one will struggle to get a large enough signal. As one would then expect, the best final state to look for is not $2b2\tau$ as was used before, but rather $4b$ which gives the highest signal rate. This is clearly seen in figure 6, where the sensitivity in the various channels are shown for 3000/fb of integrated luminosity. All channels use $m_{H_i} = 125$ GeV and the corresponding cut on the total final state invariant mass.

6.1 H_1 SM-like

Similarly to the VBF case, the SM-like H_1 scenario is difficult with respect to detection. In figure 7(a) we show the sensitivity in the $H_1 \rightarrow A_1 A_1$ channel, given $m_{H_1} = 125$ GeV (with a corresponding cut on the four-body invariant mass), as compared to the acceptable parameter points. We notice that the prospects are even dimmer than in the VBF case, basically our only hope is the jet substructure methods that gives a rather large improvement for low m_{A_1} , for the $4b$ final state used here this improvement can be significantly larger than for the $2b2\tau$ used in the VBF channels. As usual only the analysis

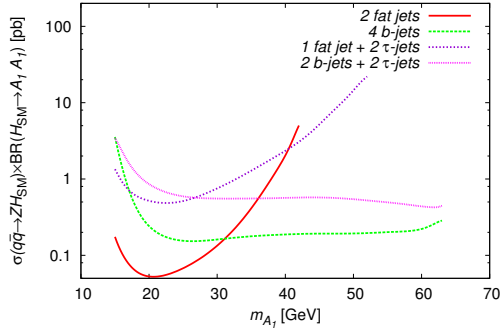


Figure 6: Sensitivity for HS off a Z boson. All curves assume 3000/fb of integrated luminosity and use $m_{H_i} = 125$ GeV and the corresponding cut on the total final state invariant mass.

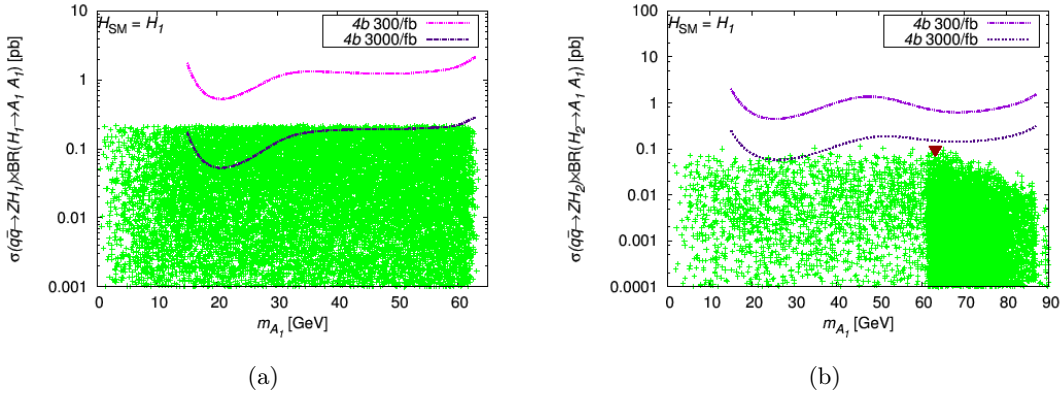


Figure 7: LHC reach in $H_1 \rightarrow A_1 A_1$ (left) and $H_2 \rightarrow A_1 A_1$ (right) for $H_1 = H_{SM}$ in the ZH channel. In panel (a) the sensitivity curves use $m_{H_1} = 125$ GeV, while (b) uses $m_{H_2} = 175$ GeV and both uses the best of the 4 b -jets and fat jets analyses. The colour code for the points is the same as in figure 1.

with the best sensitivity is used in each point of the curves.

Moving on to $H_2 \rightarrow A_1 A_1$, we see in figure 7(b) that there is only marginal hope for detection even at 3000/fb. The curves here correspond to $m_{H_2} = 175$ GeV, with no cut on the total final state invariant mass and always using the most efficient of the single b -jets/fat jets analyses. The main reason for the difficulties in this channel is clearly the small signal rates, but also the absence of a cut on the overall invariant mass impacts negatively on the sensitivity.

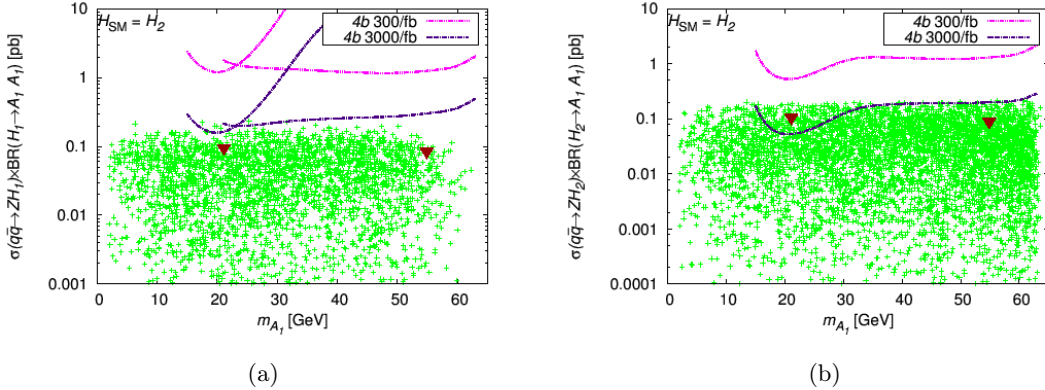


Figure 8: LHC reach in $H_1 \rightarrow A_1 A_1$ (left) and $H_2 \rightarrow A_1 A_1$ (right) for $H_2 = H_{\text{SM}}$ in the ZH channel. The sensitivity curves in panel (a) correspond to the two fat jets (the curves at low m_{A_1} using $m_{H_1} = 100$ GeV) and the four single b -jets (the curves at higher m_{A_1} using $m_{H_1} = 125$ GeV) analyses. In panel (b) $m_{H_2} = 125$ GeV is used along with the best of the 4 b -jets and fat jets analyses. The colour code for the points is the same as in figure 1.

6.2 H_2 SM-like

With the lower sensitivity as compared to VBF production, the $H_2 = H_{\text{SM}}$ is also rather difficult. As can be seen for $H_1 \rightarrow A_1 A_1$ in figure 8(a) — where the sensitivity curves use $m_{H_1} = 100$ GeV with jet substructure, and $m_{H_1} = 125$ GeV with single b -jets (no constraint on overall invariant mass), respectively — even 3000/fb is probably not sufficient for any discovery.

In figure 8(b) we show the reach for $H_2 \rightarrow A_1 A_1$, the sensitivity curves correspond to $m_{H_2} = 125$ GeV and the corresponding constrain on the four-body invariant mass, always showing the most sensitive analysis. As before, this is basically identical to figure 7(a), with only marginal discoverability for low masses where jet substructure may be useful.

7 Higgs-strahlung via WH

In general WH production will have higher cross sections than ZH production and, since the W also has roughly three times higher leptonic BR as compared to the Z , this channel will exhibit much higher rates. In order to tag the W we require exactly one isolated lepton in the event, in addition to the signal objects. Similarly to ZH production, we only look at the channel with the highest rate, i.e., $W + 4b$.

There has been a number of earlier studies of the $W + 4b$ channel, including parton level studies [89] and [90] and a full detector study in [91]. While the parton level analysis of [90] arrived at significantly higher sensitivity than we did, our results are in reasonable

agreement with [91]. (Note however that, although both of these studies use four b -tags as well as a cut on the four-body invariant mass, neither of them uses the requirement that both A_1 candidates should have similar mass.)

In addition to the irreducible $W + 4b$ background, there are significant backgrounds from $t\bar{t}$ — with two light jets from one of the resulting W s being mistagged as b -jets — as well as from $t\bar{t}b\bar{b}$ events. The latter is in our studies the most significant one, often at least one order of magnitude larger than the irreducible background. This conclusion is in agreement with [90], while [91] finds that detector smearing pushes the $t\bar{t}$ background to lower invariant masses and hence becomes a significant background also at 125 GeV. To suppress the $t\bar{t}b\bar{b}$ background we employ a veto against hadronically decaying W s. This means an event with two light jets with $p_T > 15$ GeV and combined invariant mass = 80 ± 15 GeV is rejected as it is likely to come from a $t\bar{t}b\bar{b}$ event with one W decaying leptonically and the other one hadronically. The events where both W s decay leptonically should be suppressed by the fact that we ask for exactly one lepton and hence reject events with two isolated leptons (this also suppresses any $Z + 4b$ backgrounds).

Since the smallness of the signal rates in both WH and (even more) in ZH production is a bigger problem than background suppression, one could consider requiring only three b -tags. This was the approach of [89] and should yield significantly higher signal rates, especially as one b -jet is often missed due to p_T cuts, etc. However, this requires a much more detailed study as there are many more contributing sources of background. It is also not clear how to implement the invariant mass constraints as one has to assume that sometimes the fourth b -jet is not selected even as a light jet. Such considerations are therefore beyond the scope of this paper.

7.1 H_1 SM-like

In this case higher rates as compared to ZH production does mean better discovery prospects even though the background is also larger due to $t\bar{t}b\bar{b}$.

In figure 9(a) we show the discovery reach in the $H_1 \rightarrow A_1 A_1$ channel in the $H_1 = H_{\text{SM}}$ case. The sensitivity curves are set for $m_{H_1} = 125$ GeV and the corresponding cut on the overall invariant mass. If we compare with figure 7(a), the reach here is much greater, even 300/fb might be enough for detecting some A_1 s around 20 GeV. Such a discovery is not possible even for VBF production, as can be seen in figure 4(a), where 300/fb does not reach the upper 1 pb limit for the rate. The reason for the relative success of WH production for these low masses is that in the $4b$ final state the use of fat jets leads to a more significant improvement over a single b -jet analysis than is the case for the $2b2\tau$ channel used for VBF production. Also, the backgrounds in the WH channels are more severe at higher masses, rendering the low mass region more interesting.

The $H_2 \rightarrow A_1 A_1$ channel is much less optimistic, as can be seen in figure 9(b), where we set $m_{H_2} = 175$ GeV with no cut on overall invariant mass for the sensitivity curves. It is clear the growth of the $t\bar{t}b\bar{b}$ and $t\bar{t}$ backgrounds with increasing invariant masses suppresses

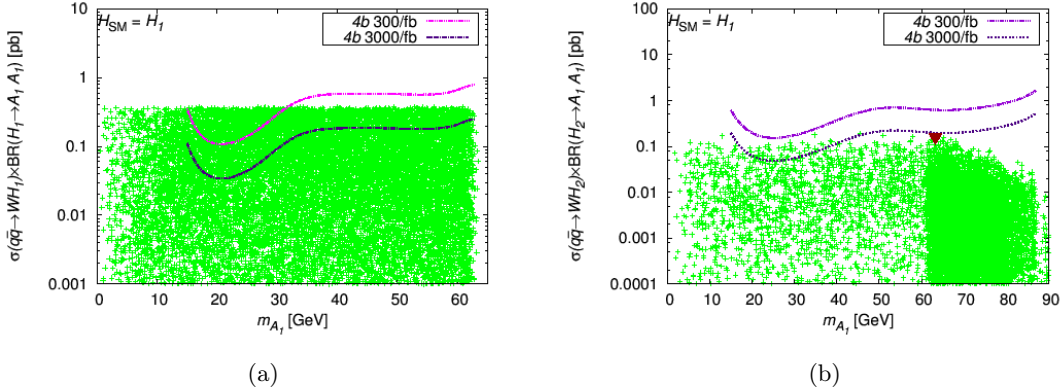


Figure 9: LHC reach in $H_1 \rightarrow A_1 A_1$ (left) and $H_2 \rightarrow A_1 A_1$ (right) for $H_1 = H_{\text{SM}}$ in the WH channel. In panel (a) the sensitivity curves use $m_{H_1} = 125$ GeV, while (b) uses $m_{H_2} = 175$ GeV and both uses the best of the 4 b -jets and fat jets analyses. The colour code for the points is the same as in figure 1.

the sensitivity at higher masses. One could try some invariant mass cuts to suppress these backgrounds and possibly reach the points just above the $m_{A_1} = m_{H_1}/2$ threshold, but we leave such considerations to section 8.

7.2 H_2 SM-like

The case $H_2 = H_{\text{SM}}$ is rather similar to the $H_1 = H_{\text{SM}}$ case. As can be seen in figure 10(a) — displaying sensitivity curves with $m_{H_1} = 100$ GeV (using fat jets) and 125 GeV (using b -jets) but with no overall cut on invariant mass — there is just a marginal hope for detection in $H_1 \rightarrow A_1 A_1$ at 3000/fb. We do see improved sensitivity in the low mass region as compared to VBF production, but not enough to cover any significant part of the parameter space. This is again a consequence of the strength of the fat jet analysis for $4b$ as well as the main backgrounds $t\bar{t}b\bar{b}$ and $t\bar{t}$ being smaller for lower invariant masses.

For $H_2 \rightarrow A_1 A_1$ (figure 10(b)) we again see essentially the same as figure 9(a). Here we use $m_{H_2} = 125$ GeV and constrain the four-body invariant mass of the final state to be 125 ± 30 GeV. The sensitivity curves use a combination of the fat jet and the single b -jet analyses, always showing the more sensitive one.

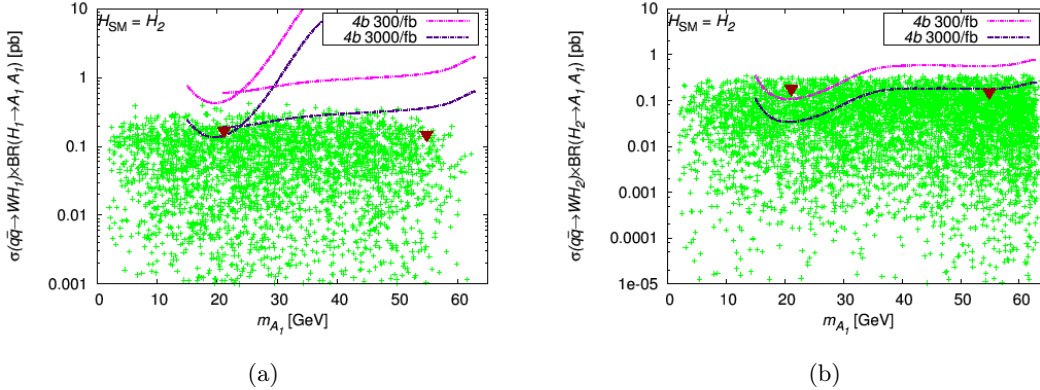


Figure 10: LHC reach in $H_1 \rightarrow A_1 A_1$ (left) and $H_2 \rightarrow A_1 A_1$ (right) for $H_2 = H_{\text{SM}}$ in the WH channel. The sensitivity curves in panel (a) correspond to the two fat jets (the curves at low m_{A_1} using $m_{H_1} = 100$ GeV) and the four single b -jets (the curves at higher m_{A_1} using $m_{H_1} = 125$ GeV) analyses. In panel (b) $m_{H_2} = 125$ GeV is used along with the best of the 4 b -jets and fat jets analyses. The colour code for the points is the same as in figure 1.

8 Benchmark points

As mentioned before, the detection sensitivities in all the channels studied in this paper are significantly worse than the corresponding results from GF production.³ Furthermore, this is generally true for all parameter space regions that we have been able to access in the analyses carried out here. Therefore it is fair to assume that, by the time the channels under investigation become interesting for experimental study, the lightest scalar (H_1 and H_2) as well as pseudoscalar (A_1) Higgs states will already have been discovered via GF and the goal for both the VBF and HS channels will become to enable one further study their properties, as explained in the introduction.

For this purpose we define three benchmark points and study them under the assumption that we know the masses involved and can hence use this information to further constrain the kinematics in the attempt to increase the sensitivity.⁴ The details of the three points are given in table 3. The points are chosen to cover as much as possible of the parameter space within reach. Point 1 has a rather light A_1 of 21 GeV and hence lies in the region where jet substructure methods are of importance, while point 2 is closer to the threshold for $H_{1,2} \rightarrow A_1 A_1$ with $m_{A_1} = 55$ GeV. The last point is the only one with $H_1 = H_{\text{SM}}$

³This is true unless the triggering in the GF channel turns out to be more challenging than what is presently hoped for.

⁴Even without prior knowledge of the masses, these analyses can be employed by scanning over the masses involved. This, however, would render large look-elsewhere effects.

Case	$H_{\text{SM}} = H_2$		$H_{\text{SM}} = H_1$
	Point 1	Point 2	Point 3
Input parameters			
m_0 (GeV)	1516.0	1470.5	1326.7
$m_{1/2}$ (GeV)	491.58	947.19	369.23
A_0 (GeV)	-2966.1	2523.0	2839.5
μ_{eff} (GeV)	113.54	122.98	189.28
$\tan \beta$	13.051	12.46	2.882
λ	0.08899	0.1641	0.5408
κ	0.04042	0.07769	0.1818
A_λ (GeV)	781.94	1714.9	479.29
$M_{p,}$ (GeV)	21.77	59.38	68.52
Observables			
m_{A_1} (GeV)	21.12	54.87	63.26
m_{H_1} (GeV)	100.54	110.77	125.45
m_{H_2} (GeV)	125.22	125.31	138.90

Table 3: Some specifics of the three benchmark points.

and with $m_{A_1} = 63$ GeV, it is designed for $H_2 \rightarrow A_1 A_1$ studies. Below the $H_{\text{SM}} \rightarrow A_1 A_1$ threshold, the phenomenology of $H_1 = H_{\text{SM}}$ and $H_2 = H_{\text{SM}}$ is very similar, obviating any need for additional benchmark points in that region.

In the study of these benchmark points we therefore use a somewhat modified kinematic analysis. Specifically, all A_1 candidates (i.e., b -jet pairs, fat jets or τ -jet pairs) are required to be within 15 GeV off the (assumed known) A_1 mass. For each point we run two simulations, one for $H_1 \rightarrow A_1 A_1$ and one for $H_2 \rightarrow A_1 A_1$ and in each case the combined invariant mass of the two A_1 candidates is required to be within 30 GeV of the (assumed known) H_1 or H_2 mass.

The result of these studies are displayed in table 4, where the cross sections after all cuts are presented for the signal as well as the backgrounds. We also show the integrated luminosity needed to obtain $S/\sqrt{B} > 5$ with at least 10 events. The result of the jet substructure (fat jet) analysis is only shown for point 1 as this is the only scenario with an A_1 light enough for such studies to be useful, though, in that case, this is clearly the most effective approach. Also, we do not include $H_1 \rightarrow A_1 A_1$ for point 3 as this channel is kinematically closed.

As stated before, the signals are in general larger than the backgrounds and, in many cases, the main constraint on the required luminosity is the requirement of at least 10 events. We also see in table 4 that WH is usually the most promising channel as it has the highest rates. It also has the highest backgrounds though, due to $t\bar{t}b\bar{b}$ and $t\bar{t}$ and, since

	Point 1				Point 2		Point 3
	$H_i = H_1$		$H_i = H_2$		$H_i = H_1$	$H_i = H_2$	$H_i = H_2$
	b -jets	fat jet	b -jets	fat jet	b -jets	b -jets	b -jets
$q\bar{q}H_i \rightarrow q\bar{q}2b2\tau$							
Signal [pb]	1.7×10^{-6}	2.7×10^{-6}	4.1×10^{-6}	8.8×10^{-6}	3.9×10^{-6}	7.0×10^{-6}	1.0×10^{-5}
$2j + 2b2\tau$	2.4×10^{-7}	8.5×10^{-7}	2.4×10^{-7}	8.5×10^{-7}	2.6×10^{-6}	2.6×10^{-6}	3.4×10^{-6}
$2j + t\bar{t}$	6.8×10^{-7}	2.2×10^{-6}	6.8×10^{-7}	2.2×10^{-7}	1.1×10^{-6}	1.1×10^{-6}	1.5×10^{-6}
\mathcal{L} [fb $^{-1}$]	8400	10000	2400	1100	5800	1900	1200
$ZH_i \rightarrow 2\ell 4b$							
Signal [pb]	1.4×10^{-6}	4.1×10^{-6}	2.9×10^{-6}	7.8×10^{-6}	2.2×10^{-6}	2.9×10^{-6}	4.0×10^{-6}
$Z + 4b$ [pb]	9.1×10^{-7}	1.1×10^{-6}	8.7×10^{-7}	1.1×10^{-6}	2.7×10^{-6}	3.9×10^{-6}	4.0×10^{-6}
\mathcal{L} [fb $^{-1}$]	11000	2400	3500	1300	13000	11000	6300
$WH_i \rightarrow \ell 4b$							
Signal [pb]	1.1×10^{-5}	3.9×10^{-5}	2.1×10^{-5}	7.3×10^{-5}	1.5×10^{-5}	2.0×10^{-5}	2.7×10^{-5}
$W + 4b$ [pb]	1.1×10^{-6}	1.7×10^{-6}	9.3×10^{-7}	1.7×10^{-6}	2.2×10^{-6}	2.8×10^{-6}	2.5×10^{-6}
$t\bar{t}b\bar{b}$ [pb]	8.2×10^{-6}	1.4×10^{-5}	7.5×10^{-6}	1.8×10^{-5}	3.1×10^{-5}	4.5×10^{-5}	4.2×10^{-5}
$t\bar{t}$ [pb]	9.3×10^{-7}	4.9×10^{-7}	1.3×10^{-6}	6.9×10^{-7}	4.3×10^{-6}	7.7×10^{-6}	1.1×10^{-5}
\mathcal{L} [fb $^{-1}$]	2300	266	548	138	3900	3400	1900

Table 4: Discovery prospects for the three benchmark points. \mathcal{L} denotes the integrated luminosity required for a detection in the given channel.

these tend to increase with increasing H_i mass, we note that for $H_2 \rightarrow A_1 A_1$ in point 2 and 3 the VBF channel is somewhat better.

Comparing the detection prospects in table 4, with the reach shown in the corresponding plots, it is clear that the additional constraints on the kinematics due to the assumption about the mass spectrum are important in improving sensitivity, though in some cases the differences are negligible. The invariant mass cuts are especially important for WH as the $t\bar{t}b\bar{b}$ and $t\bar{t}$ backgrounds increase significantly with increasing overall invariant mass, hence rendering a (relatively low) cut on over all invariant mass very effective.

To illustrate more clearly the signal and backgrounds in the WH channels we plot these as functions of the invariant mass of the b -jet pairs⁵, m_{bb} , in figure 11 for $H_1 \rightarrow A_1 A_1$ in point 1 (figure 11(a)) and for $H_2 \rightarrow A_1 A_1$ in point 3 (figure 11(b)). Note that, due to the cuts in the analysis, the distributions are restricted to $m_{bb} \pm 15$ GeV and that both plots use single b -jet analysis only. In figure 11(a) it is clear that a somewhat narrower cut would significantly reduce the background from $t\bar{t}b\bar{b}$ without affecting the signal significantly. However, it is important to note that there are significant statistical uncertainties in the backgrounds (partially hidden by the smoothing) and this, together with the fact that the signal already dominates and that we do not include detector resolution, means that

⁵Included here are the two invariant masses of the combination of b -jet pairs that have the smallest difference in invariants mass of all the combinations of b -jet pairs where both pairs have invariant mass within $m_{A_1} \pm 15$ GeV.

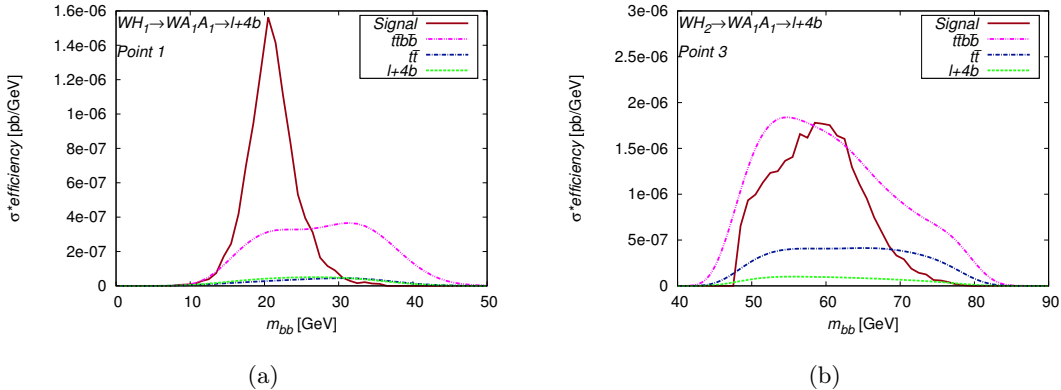


Figure 11: Signal and backgrounds for two of our benchmark points in the WH channel. The backgrounds have been smoothed for visual clarity.

it is not clear how beneficial such a cut would really be. From figure 11(b) we see that for heavier masses the invariant mass peak is smeared out towards smaller masses, this is mostly an effect of the difficulty in finding the “right” b -jet pairs; for lighter A_1 s the “wrong” pairing gives too high invariant masses to be included.

9 Prospects at Higgs factories

Since we have seen that the conditions for detecting light pseudoscalars at the LHC via VBF and HS are rather challenging and it may require several years to do so, it is worth investigating whether a Higgs factory would do better in this respect. To this end, we estimate the sensitivity of a 240 GeV e^+e^- collider that produces CP-even Higgses primarily through the ZH channel. Since the hadronic background here is much smaller than at the LHC, we do not require any b -tagging but just look for a leptonically decaying Z -boson (into electrons/muons) accompanied by exactly 4 jets (each with $p_T > 15$ GeV).

In all other aspects our analysis is identical to what was done for the LHC, except that we do not include jet substructure techniques at this point. In fact, we only study chains starting with H_{SM} for which we assume a production cross section of $\sigma(e^+e^- \rightarrow H_{\text{SM}}Z) = 200$ fb. The resulting sensitivity is shown in figure 12. It is clear that a Higgs factory would be much more suitable for our channels, as sensitivity to the NMSSM dynamics will be established already in the first year of operation. Furthermore, the very low background also means that profiling the events in terms of underlying mass spectra and $H_{\text{SM}}WW$ coupling strength would be an easier task than at the LHC.

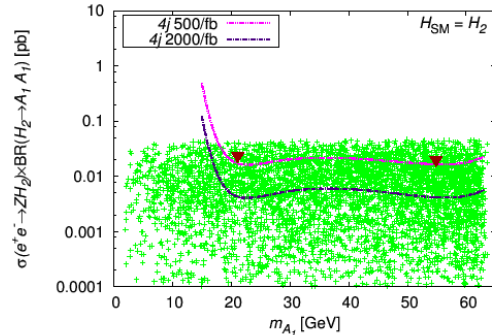


Figure 12: Reach of a 240 GeV e^+e^- collider in $H_2 \rightarrow A_1A_1$ for $H_2 = H_{\text{SM}}$ in the ZH channel. All sensitivity curves assumes $m_{H_2} = 125$ GeV and looks for four jets with total invariant mass of 125 GeV in addition to the leptonically decaying Z . The colour code for the points is the same as in figure 1.

10 Conclusions

In contrast to the more constrained MSSM, the NMSSM allows for the existence of very light Higgs scalars as well as pseudoscalars. Therefore, the discovery of, in particular, a light pseudoscalar Higgs state would not just prove the existence of physics beyond the SM but would also be inconsistent with minimal supersymmetry.

Since the NMSSM also accommodates the 125 GeV Higgs more naturally than the MSSM, it is well worth a study. Although the most promising LHC discovery channels of the aforementioned light pseudoscalar state are most likely based on GF production of heavier scalars that subsequently decay to A_1A_1 or A_1Z , we demonstrated here that also VBF and HS production of the heavier scalars can be accessible. Hence, these two additional production modes can be exploited to study couplings not accessible in GF, such as those of the heavy scalars to SM gauge bosons. Especially interesting are the channels starting with H_S : as these can have $\text{BR}(H_i \rightarrow A_1A_1)$ close to 1, the channels of this paper might be our only chance of measuring the couplings of these scalars to gauge bosons.

In these channels, the signal rates are substantially lower than in the case of GF, but the same is true for the backgrounds. Due to the nature of the couplings involved, the only decay chains of interest here are $H_{1,2} \rightarrow A_1A_1$. For VBF production of $H_{1,2}$ the most promising of our final states is $2b2\tau$ (in addition to the two forward/backward jets), which may allow detection, although only at 3000/fb.

For HS production, the background is even smaller, especially for the ZH mode. However, this channel also has a very small cross section and hence the signal will be very hard to extract. As the event rates are indeed significantly smaller compared to VBF and GF, here it is most beneficial to employ the final state with the highest rate, i.e., $4b$.

Although still featuring a relatively low signal rate, WH production shows significantly

better prospects than ZH . Despite significant backgrounds from $t\bar{t}b\bar{b}$ and $t\bar{t}$, the higher signal rates make this the most promising channel studied in this paper, at least for relatively light initial scalars. However, given the invariant mass structure of the main backgrounds, the signal tends to be overwhelmed unless one can cut on the four- b invariant mass and the enforced mass window needs to be relatively narrow. Therefore, the prospects for this channel diminish as the mass of the initially produced scalar increases, rendering VBF the most promising channel for heavier scalars.

In addition to general scans for sensitivity reach in parameter space, we have performed more detailed studies of three representative benchmark points. Here, we assumed knowledge of the masses of the produced scalar as well as the pseudoscalar (e.g., as measured in GF production) and used this information to constrain the kinematics. Especially for HS, this can dramatically improve the sensitivity.

Finally, we have briefly tested how the LHC prospects compare to those of a future e^+e^- machine running at the threshold of ZH production, the golden (Bjorken in this case) channel of such a Higgs factory. Needless to say, sensitivity to $H_{\text{SM}} \rightarrow A_1 A_1$ decays is rather prompt herein. Further, the clean environment of an e^+e^- machine in terms of very limited backgrounds will enable precise diagnostic of the NMSSM dynamics involved. It remain to be seen whether commissioning of such a leptonic machine will occur on a timescale that will make it competitive with a potential LHC stage at high (instantaneous) luminosity, the so-called Super-LHC (SLHC) option [92], currently being discussed as a probable upgrade of the CERN collider past Run II.

Acknowledgments

We would like to thank Shoaib Munir and Robin Aggleton for useful discussions. This work has been funded in part by the Welcome Programme of the Foundation for Polish Science. S. Moretti is supported in part through the NExT Institute. L. Roszkowski is also supported in part by a Lancaster-Manchester-Sheffield Consortium for Fundamental Physics under STFC grant ST/L000520/1. The use of the CIS computer cluster at NCBJ is gratefully acknowledged.

References

- [1] U. Ellwanger, C. Hugonie, and A. M. Teixeira, *Phys.Rept.* **496**, 1 (2010), 0910.1785.
- [2] ATLAS Collaboration, G. Aad *et al.*, *Phys.Lett.* **B716**, 1 (2012), 1207.7214.
- [3] CMS Collaboration, S. Chatrchyan *et al.*, *Phys.Lett.* **B716**, 30 (2012), 1207.7235.
- [4] CLEO Collaboration, W. Love *et al.*, *Phys.Rev.Lett.* **101**, 151802 (2008), 0807.1427.
- [5] E391a Collaboration, Y. Tung *et al.*, *Phys.Rev.Lett.* **102**, 051802 (2009), 0810.4222.

- [6] BaBar collaboration, J. Lees *et al.*, Phys.Rev. **D87**, 031102 (2013), 1210.0287.
- [7] BaBar Collaboration, J. Lees *et al.*, Phys.Rev. **D88**, 071102 (2013), 1210.5669.
- [8] BaBar Collaboration, J. Lees *et al.*, Phys.Rev. **D88**, 031701 (2013), 1307.5306.
- [9] BABAR Collaboration, I. Peruzzi, EPJ Web Conf. **71**, 00108 (2014).
- [10] OPAL Collaboration, G. Abbiendi *et al.*, Eur.Phys.J. **C27**, 483 (2003), hep-ex/0209068.
- [11] ALEPH Collaboration, S. Schael *et al.*, JHEP **1005**, 049 (2010), 1003.0705.
- [12] D0 Collaboration, V. Abazov *et al.*, Phys.Rev.Lett. **103**, 061801 (2009), 0905.3381.
- [13] CMS Collaboration, S. Chatrchyan *et al.*, Phys.Rev.Lett. **109**, 121801 (2012), 1206.6326.
- [14] CMS Collaboration, S. Chatrchyan *et al.*, Phys.Lett. **B726**, 564 (2013), 1210.7619.
- [15] CMS, V. Khachatryan *et al.*, JHEP **01**, 079 (2016), 1510.06534.
- [16] CMS, V. Khachatryan *et al.*, Phys. Lett. **B750**, 494 (2015), 1506.02301.
- [17] CMS, V. Khachatryan *et al.*, Phys. Lett. **B749**, 560 (2015), 1503.04114.
- [18] ATLAS Collaboration, G. Aad *et al.*, Phys.Rev.Lett. **113**, 171801 (2014), 1407.6583.
- [19] J. Dai, J. Gunion, and R. Vega, Phys.Lett. **B315**, 355 (1993), hep-ph/9306319.
- [20] U. Ellwanger, JHEP **1308**, 077 (2013), 1306.5541.
- [21] E. Accomando *et al.*, (2006), hep-ph/0608079.
- [22] M. Almarashi and S. Moretti, Eur.Phys.J. **C71**, 1618 (2011), 1011.6547.
- [23] M. Almarashi and S. Moretti, Phys.Rev. **D84**, 015014 (2011), 1105.4191.
- [24] U. Ellwanger, J. F. Gunion, and C. Hugonie, JHEP **0507**, 041 (2005), hep-ph/0503203.
- [25] U. Ellwanger, J. F. Gunion, C. Hugonie, and S. Moretti, (2003), hep-ph/0305109.
- [26] U. Ellwanger, J. F. Gunion, and C. Hugonie, p. 178 (2001), hep-ph/0111179.
- [27] C. Hugonie and S. Moretti, eConf **C010630**, P108 (2001), hep-ph/0110241.
- [28] A. Belyaev *et al.*, (2008), 0805.3505.

- [29] J. Forshaw, J. Gunion, L. Hodgkinson, A. Papaefstathiou, and A. Pilkington, *JHEP* **0804**, 090 (2008), 0712.3510.
- [30] A. Belyaev, J. Pivarski, A. Safonov, S. Senkin, and A. Tatarinov, *Phys.Rev.* **D81**, 075021 (2010), 1002.1956.
- [31] S. Moretti and S. Munir, *Eur.Phys.J.* **C47**, 791 (2006), hep-ph/0603085.
- [32] S. Moretti, S. Munir, and P. Poulose, *Phys.Lett.* **B644**, 241 (2007), hep-ph/0608233.
- [33] M. M. Almarashi and S. Moretti, *Phys.Rev.* **D83**, 035023 (2011), 1101.1137.
- [34] U. Ellwanger and C. Hugonie, *Eur.Phys.J.* **C25**, 297 (2002), hep-ph/9909260.
- [35] A. Djouadi *et al.*, *JHEP* **0807**, 002 (2008), 0801.4321.
- [36] F. Mahmoudi, J. Rathsman, O. Stål, and L. Zeune, *Eur.Phys.J.* **C71**, 1608 (2011), 1012.4490.
- [37] R. Dermisek and J. F. Gunion, *Phys.Rev.Lett.* **95**, 041801 (2005), hep-ph/0502105.
- [38] J. F. Gunion, H. E. Haber, and T. Moroi, *eConf* **C960625**, LTH095 (1996), hep-ph/9610337.
- [39] B. A. Dobrescu, G. L. Landsberg, and K. T. Matchev, *Phys.Rev.* **D63**, 075003 (2001), hep-ph/0005308.
- [40] U. Ellwanger, J. Gunion, C. Hugonie, and S. Moretti, (2004), hep-ph/0401228.
- [41] M. Lisanti and J. G. Wacker, *Phys.Rev.* **D79**, 115006 (2009), 0903.1377.
- [42] M. Almarashi and S. Moretti, *Phys.Rev.* **D84**, 035009 (2011), 1106.1599.
- [43] M. M. Almarashi and S. Moretti, *Phys.Rev.* **D85**, 017701 (2012), 1109.1735.
- [44] M. M. Almarashi and S. Moretti, (2012), 1205.1683.
- [45] S. King, M. Mühlleitner, R. Nevzorov, and K. Walz, *Phys.Rev.* **D90**, 095014 (2014), 1408.1120.
- [46] J. E. Kim, H. P. Nilles, and M.-S. Seo, *Mod.Phys.Lett.* **A27**, 1250166 (2012), 1201.6547.
- [47] S. Munir, L. Roszkowski, and S. Trojanowski, *Phys. Rev.* **D88**, 055017 (2013), 1305.0591.
- [48] J. Kozaczuk and T. A. W. Martin, *JHEP* **04**, 046 (2015), 1501.07275.

- [49] N.-E. Bomark, S. Moretti, S. Munir, and L. Roszkowski, JHEP **1502**, 044 (2015), 1409.8393.
- [50] D. G. Cerdeno, P. Ghosh, and C. B. Park, JHEP **1306**, 031 (2013), 1301.1325.
- [51] D. Curtin, R. Essig, and Y.-M. Zhong, JHEP **06**, 025 (2015), 1412.4779.
- [52] O. Stål and G. Weiglein, JHEP **1201**, 071 (2012), 1108.0595.
- [53] D. Das, U. Ellwanger, and A. M. Teixeira, JHEP **1204**, 067 (2012), 1202.5244.
- [54] D. G. Cerdeño, P. Ghosh, C. B. Park, and M. Peiró, JHEP **1402**, 048 (2014), 1307.7601.
- [55] S. King, M. Mühlleitner, R. Nevzorov, and K. Walz, Nucl.Phys. **B870**, 323 (2013), 1211.5074.
- [56] N.-E. Bomark, S. Moretti, S. Munir, and L. Roszkowski, PoS **Charged2014**, 029 (2015), 1412.5815.
- [57] N.-E. Bomark, S. Moretti, S. Munir, and L. Roszkowski, (2015), 1502.05761.
- [58] D. Curtin *et al.*, Phys.Rev. **D90**, 075004 (2014), 1312.4992.
- [59] U. Ellwanger, JHEP **1203**, 044 (2012), 1112.3548.
- [60] S. King, M. Mühlleitner, and R. Nevzorov, Nucl.Phys. **B860**, 207 (2012), 1201.2671.
- [61] U. Ellwanger and C. Hugonie, Adv.High Energy Phys. **2012**, 1 (2012), 1203.5048.
- [62] T. Gherghetta, B. von Harling, A. D. Medina, and M. A. Schmidt, JHEP **1302**, 032 (2013), 1212.5243.
- [63] J. Cao *et al.*, JHEP **1203**, 086 (2012), 1202.5821.
- [64] K. S. Jeong, Y. Shoji, and M. Yamaguchi, JHEP **1209**, 007 (2012), 1205.2486.
- [65] K. Agashe, Y. Cui, and R. Franceschini, JHEP **1302**, 031 (2013), 1209.2115.
- [66] R. Barbieri, D. Buttazzo, K. Kannike, F. Sala, and A. Tesi, Phys. Rev. D 87, **115018** (2013), 1304.3670.
- [67] M. Badziak, M. Olechowski, and S. Pokorski, JHEP **1306**, 043 (2013), 1304.5437.
- [68] R. Barbieri, D. Buttazzo, K. Kannike, F. Sala, and A. Tesi, Phys.Rev. **D88**, 055011 (2013), 1307.4937.

- [69] F. Feroz, M. Hobson, and M. Bridges, *Mon.Not.Roy.Astron.Soc.* **398**, 1601 (2009), 0809.3437.
- [70] <http://www.th.u-psud.fr/NMHDECAY/nmssmtools.html>.
- [71] P. Bechtle, O. Brein, S. Heinemeyer, G. Weiglein, and K. E. Williams, *Comput.Phys.Commun.* **181**, 138 (2010), 0811.4169.
- [72] P. Bechtle, O. Brein, S. Heinemeyer, G. Weiglein, and K. E. Williams, *Comput.Phys.Commun.* **182**, 2605 (2011), 1102.1898.
- [73] P. Bechtle *et al.*, *PoS CHARGED2012*, 024 (2012), 1301.2345.
- [74] P. Bechtle *et al.*, *Eur.Phys.J.* **C74**, 2693 (2014), 1311.0055.
- [75] A. Arbey and F. Mahmoudi, *Comput.Phys.Commun.* **176**, 367 (2007), 0906.0369.
- [76] Particle Data Group, J. Beringer *et al.*, *Phys.Rev.* **D86**, 010001 (2012).
- [77] Planck Collaboration, P. Ade *et al.*, *Astron.Astrophys.* **571**, A16 (2014), 1303.5076.
- [78] G. Belanger, F. Boudjema, A. Pukhov, and A. Semenov, *Comput.Phys.Commun.* **181**, 1277 (2010), hep-ph/0607059.
- [79] CMS, V. Khachatryan *et al.*, *Eur. Phys. J.* **C75**, 212 (2015), 1412.8662.
- [80] ATLAS, G. Aad *et al.*, *Phys.Rev.* **D90**, 052004 (2014), 1406.3827.
- [81] J. Bernon, B. Dumont, and S. Kraml, *Phys. Rev.* **D90**, 071301 (2014), 1409.1588.
- [82] J. Alwall *et al.*, *JHEP* **1407**, 079 (2014), 1405.0301.
- [83] T. Sjöstrand, S. Mrenna, and P. Z. Skands, *Comput.Phys.Commun.* **178**, 852 (2008), 0710.3820.
- [84] M. Cacciari, G. P. Salam, and G. Soyez, *Eur.Phys.J.* **C72**, 1896 (2012), 1111.6097.
- [85] LHC Higgs Cross Section Working Group, S. Dittmaier *et al.*, (2011), 1101.0593.
- [86] CMS Collaboration, CERN Report No. CMS-DP-2014-015, 2014 (unpublished).
- [87] CMS Collaboration, CERN Report No. CMS-PAS-BTV-13-001, 2013 (unpublished).
- [88] J. M. Butterworth, A. R. Davison, M. Rubin, and G. P. Salam, *Phys.Rev.Lett.* **100**, 242001 (2008), 0802.2470.
- [89] M. Carena, T. Han, G.-Y. Huang, and C. E. Wagner, *JHEP* **0804**, 092 (2008), 0712.2466.

- [90] K. Cheung, J. Song, and Q.-S. Yan, Phys.Rev.Lett. **99**, 031801 (2007), hep-ph/0703149.
- [91] J. Cao, F. Ding, C. Han, J. M. Yang, and J. Zhu, JHEP **1311**, 018 (2013), 1309.4939.
- [92] F. Gianotti *et al.*, Eur. Phys. J. **C39**, 293 (2005), hep-ph/0204087.